NUCLEAR THEORY, Vol. 41 (2024)
eds. M. Gaidarov, N. Minkov, Heron Press, Sofia

Analysis of Elastic Scattering Observables Calculated with Different NN Interactions

G. Popa[1], **R.B. Baker**[1], **M. Burrows**[2], **Ch. Elster**[1], **P. Maris**[3], **S.P. Weppner**[4]

[1]Institute of Nuclear and Particle Physics, and Department of Physics and Astronomy, Ohio University, Athens, Ohio 45701, USA
[2]Department of Physics and Astronomy, Louisiana State University, Baton Rouge, Louisiana 70803, USA
[3]Department of Physics and Astronomy, Iowa State University, Ames, Iowa 50011, USA
[4]Natural Sciences, Eckerd College, St. Petersburg, Florida 33711, USA

Abstract. Nuclear scattering experiments have been used to provide detailed information about the structure of nuclei for decades. They help in understanding the behavior of neutrons and protons within the nucleus, and provide insights into the energy levels, spin states, and magnetic moments of nucleons, which are important for nuclear physics and applications in reactor design and nuclear medicine. Understanding nucleon-nucleus interactions is vital for interpreting processes in stellar environments and supernovae.

We calculated and present nucleon-nucleus effective interactions and elastic scattering observables in the leading-order spectator expansion for closed and open shell nuclei, like ^{4}He, ^{12}C, and ^{16}O, at projectile energies between 65 and 160 (180) MeV, using three different nucleon-nucleon (NN) interactions (up to next-to-next-to-leading order), based on chiral effective field theory. The one-body density matrix used in the effective interaction, has been constructed within the framework of the no-core shell model

1 Introduction

Continuous developments of nucleon-nucleon (NN) and three nucleon (3N) interactions derived from chiral effective theory [1–4] together with utilization of parallel computing resources have placed *ab initio* calculations at the frontier of structure and reactions explorations.The *ab initio* no-core shell model (NCSM) approach (see, *e.g.* [5–9]) has considerably advanced our understanding and description of low-lying states in light nuclei. One way to extend this approach to nuclear reactions is the construction of *ab initio* effective interactions for e.g. nucleon elastic scattering from nuclei in a framework based on spectator expansion [10] of multiple scattering theory.The nuclear one-body densities required for the folding with NN scattering amplitudes are based on the same chiral NN interactions.

In this work we compare calculations of radii, binding energies, and elastic scattering observables using the same framework, but employing three different NN interactions based on chiral effective field theory, calibrated to reproduce similar data in the few-nucleon sector. The three different interactions, namely the NNLO_{opt} [1] and the EKM [2], as well as the Daejeon16 potential [4] are used in calculation of one-body densities and the NN amplitudes, which are relevant for constructing the effective NA interaction.

2 Theoretical Framework

Calculating elastic nucleon-nucleus scattering observables in an *ab initio* fashion requires the interaction between the projectile and the nucleons in the target, as well as the interaction between the nucleons within the target. A multiple scattering expansion can organize the interactions between the projectile and the nucleons in the target according to the number of active nucleons participating in the reaction, as is done in the spectator expansion [10–12]. The structure of the target nucleus is calculated employing *ab initio* many-body methods. For this work we are using the no-core shell model (NCSM), which is well-suited for light nuclei.

Up to now the leading order in the spectator expansion, which implies two active nucleons, has been evaluated *ab initio* in several works for elastic scattering of protons (neutrons) from nuclei with a 0^+ ground state [14–16] as well as nuclei with $J^\pi \neq 0^+$ [17]. In this work we concentrate on proton scattering from light nuclei with $J^\pi = 0^+$ in leading order in the spectator expansion. In this case the effective interaction of the projectile proton with a single target nucleon can be written as function of the momentum transfer $\boldsymbol{q}$ and the average momentum $\boldsymbol{\mathcal{K}}_{\text{NA}}$, where the subscript NA refers to the nucleon-nucleus (NA) frame.

$$\begin{aligned}\widehat{U}_{\text{p}}(\boldsymbol{q},\boldsymbol{\mathcal{K}}_{\text{NA}};\epsilon) = &\sum_{\alpha=\text{n,p}} \int d^3\mathcal{K}\eta(\boldsymbol{\mathcal{K}},-)A_{\text{p}\alpha}(\boldsymbol{q},\boldsymbol{\mathcal{K}}_{\text{NA}},\boldsymbol{\mathcal{K}},\epsilon)\rho_\alpha^{K_s=0}(\boldsymbol{\mathcal{P}'},\boldsymbol{\mathcal{P}}) \\ &+ i(\boldsymbol{\sigma^{(0)}}\cdot\hat{\boldsymbol{n}}) \sum_{\alpha=\text{n,p}} \int d^3\mathcal{K}\eta(\boldsymbol{\mathcal{K}},-)C_{\text{p}\alpha}(\boldsymbol{q},\boldsymbol{\mathcal{K}}_{\text{NA}},\boldsymbol{\mathcal{K}},\epsilon)\rho_\alpha^{K_s=0}(\boldsymbol{\mathcal{P}'},\boldsymbol{\mathcal{P}}) \\ &+ i \sum_{\alpha=\text{n,p}} \int d^3\mathcal{K}\eta(\boldsymbol{\mathcal{K}},-)C_{\text{p}\alpha}\left(\boldsymbol{q},\boldsymbol{\mathcal{K}}_{\text{NA}},\boldsymbol{\mathcal{K}},\epsilon\right) S_{n,\alpha}(\boldsymbol{\mathcal{P}'},\boldsymbol{\mathcal{P}})\cos\beta \\ &+ i(\boldsymbol{\sigma^{(0)}}\cdot\hat{\boldsymbol{n}}) \sum_{\alpha=\text{n,p}} \int d^3\mathcal{K}\eta(\boldsymbol{\mathcal{K}},-)(-i)M_{\text{p}\alpha}(\boldsymbol{q},\boldsymbol{\mathcal{K}}_{\text{NA}},\boldsymbol{\mathcal{K}},\epsilon)S_{n,\alpha}(\boldsymbol{\mathcal{P}'},\boldsymbol{\mathcal{P}})\cos\beta, \quad (1)\end{aligned}$$

where the subscript p indicates the projectile being a proton. The energy ϵ is taken in the impulse approximation as half of the projectile energy. To shorten formula (1), the factor $\eta\left(\boldsymbol{q},\boldsymbol{\mathcal{K}},\boldsymbol{\mathcal{K}}_{\text{NA}}\right)$ is written as $\eta\left(\boldsymbol{\mathcal{K}},-\right)$,

$$A_{\mathrm{p}\alpha}\left(\boldsymbol{q}, \frac{1}{2}\left(\frac{A+1}{A}\boldsymbol{\mathcal{K}}_{\mathrm{NA}} - \boldsymbol{\mathcal{K}}\right); \epsilon\right) = A_{\mathrm{p}\alpha}\left(\boldsymbol{q}, \boldsymbol{\mathcal{K}}_{\mathrm{NA}}, \boldsymbol{\mathcal{K}}, \epsilon\right) \tag{2}$$

$$C_{\mathrm{p}\alpha}\left(\boldsymbol{q}, \frac{1}{2}\left(\frac{A+1}{A}\boldsymbol{\mathcal{K}}_{\mathrm{NA}} - \boldsymbol{\mathcal{K}}\right); \epsilon\right) = C_{\mathrm{p}\alpha}\left(\boldsymbol{q}, \boldsymbol{\mathcal{K}}_{\mathrm{NA}}, \boldsymbol{\mathcal{K}}, \epsilon\right), \quad \text{and} \tag{3}$$

$$M_{\mathrm{p}\alpha}\left(\boldsymbol{q}, \frac{1}{2}\left(\frac{A+1}{A}\boldsymbol{\mathcal{K}}_{\mathrm{NA}} - \boldsymbol{\mathcal{K}}\right); \epsilon\right) = M_{\mathrm{p}\alpha}\left(\boldsymbol{q}, \boldsymbol{\mathcal{K}}_{\mathrm{NA}}, \boldsymbol{\mathcal{K}}, \epsilon\right). \tag{4}$$

The momentum vectors are given as

$$\begin{aligned}
\boldsymbol{q} &= \boldsymbol{p'} - \boldsymbol{p} = \boldsymbol{k'} - \boldsymbol{k}, \\
\boldsymbol{\mathcal{K}} &= \frac{1}{2}\left(\boldsymbol{p'} + \boldsymbol{p}\right), \\
\hat{\boldsymbol{n}} &= \frac{\boldsymbol{\mathcal{K}} \times \boldsymbol{q}}{|\boldsymbol{\mathcal{K}} \times \boldsymbol{q}|} \\
\boldsymbol{\mathcal{K}}_{\mathrm{NA}} &= \frac{A}{A+1}\left[\left(\boldsymbol{k'} + \boldsymbol{k}\right) + \frac{1}{2}\left(\boldsymbol{p'} + \boldsymbol{p}\right)\right], \\
\boldsymbol{\mathcal{P}} &= \boldsymbol{\mathcal{K}} + \frac{A-1}{A}\frac{\boldsymbol{q}}{2}, \\
\boldsymbol{\mathcal{P}'} &= \boldsymbol{\mathcal{K}} - \frac{A-1}{A}\frac{\boldsymbol{q}}{2}.
\end{aligned} \tag{5}$$

The momentum of the incoming proton is given by $\boldsymbol{k}$, its outgoing momentum by $\boldsymbol{k'}$, the momentum transfer by $\boldsymbol{q}$, and the average momentum $\boldsymbol{\mathcal{K}}_{\mathrm{NA}}$. The struck nucleon in the target has an initial momentum $\boldsymbol{p}$ and a final momentum $\boldsymbol{p'}$. The two quantities representing the structure of the nucleus are the scalar one-body density $\rho_{\alpha}^{K_s=0}\left(\boldsymbol{\mathcal{P}'}, \boldsymbol{\mathcal{P}}\right)$ and the spin-projected momentum distribution $S_{n,\alpha}\left(\boldsymbol{\mathcal{P}'}, \boldsymbol{\mathcal{P}}\right)$. Both distributions are nonlocal and translationally invariant. Lastly, the term $\cos\beta$ in Eq. (1) comes from projecting $\hat{\boldsymbol{n}}$ from the NN frame to the NA frame. For further details see Ref. [15]. The term $\eta\left(\boldsymbol{q}, \boldsymbol{\mathcal{K}}, \boldsymbol{\mathcal{K}}_{\mathrm{NA}}\right)$ is the Møller factor [18] describing the transformation from the NN frame to the NA frame.

The leading order term of Eq. (1) does not directly enter a Lippmann-Schwinger type integral equation. To obtain the Watson optical potential $U_p(\boldsymbol{q}, \boldsymbol{\mathcal{K}}_{\mathrm{NA}}; \epsilon)$, an additional integral equation needs to be solved [12, 14],

$$U_{\mathrm{p}} = \widehat{U}_{\mathrm{p}} - \widehat{U}_{\mathrm{p}} G_0(E) P U_{\mathrm{p}}, \tag{6}$$

where for simplicity the momentum variables are omitted. Here $G_0(E)$ is the free NA propagator and P a projector on the ground state.

The functions $A_{\mathrm{p}\alpha}$, $C_{\mathrm{p}\alpha}$, and $M_{\mathrm{p}\alpha}$ represent the NN interaction through Wolfenstein amplitudes. Since the incoming proton can interact with either a proton or a neutron in the nucleus, the index α indicates the neutron (n) and proton (p) contributions, which are calculated separately and then summed up. With respect to the nucleus, the operator $i(\boldsymbol{\sigma}^{(\mathbf{0})} \cdot \hat{\boldsymbol{n}})$ represents the spin-orbit operator in momentum space of the projectile.

The effective NA interaction in the leading order spectator expansion is driven by the NN amplitude, which in its most general form can be parameterized in terms of Wolfenstein amplitudes [19],

$$\begin{aligned}\overline{M}(\boldsymbol{q},\boldsymbol{\mathcal{K}}_{\rm NN},\epsilon) &= A(\boldsymbol{q},\boldsymbol{\mathcal{K}}_{\rm NN},\epsilon)\mathbf{1}\otimes\mathbf{1}\\ &+iC(\boldsymbol{q},\boldsymbol{\mathcal{K}}_{\rm NN},\epsilon)\ \left(\boldsymbol{\sigma}^{(\mathbf{0})}\cdot\hat{\boldsymbol{n}}\right)\otimes\mathbf{1}\\ &+iC(\boldsymbol{q},\boldsymbol{\mathcal{K}}_{\rm NN},\epsilon)\ \mathbf{1}\otimes\left(\boldsymbol{\sigma}^{(\boldsymbol{i})}\cdot\hat{\boldsymbol{n}}\right)\\ &+M(\boldsymbol{q},\boldsymbol{\mathcal{K}}_{\rm NN},\epsilon)(\boldsymbol{\sigma}^{(\mathbf{0})}\cdot\hat{\boldsymbol{n}})\otimes(\boldsymbol{\sigma}^{(\boldsymbol{i})}\cdot\hat{\boldsymbol{n}})\\ &+\left[G(\boldsymbol{q},\boldsymbol{\mathcal{K}}_{\rm NN},\epsilon)-H(\boldsymbol{q},\boldsymbol{\mathcal{K}}_{\rm NN},\epsilon)\right](\boldsymbol{\sigma}^{(\mathbf{0})}\cdot\hat{\boldsymbol{q}})\otimes(\boldsymbol{\sigma}^{(\boldsymbol{i})}\cdot\hat{\boldsymbol{q}})\\ &+\left[G(\boldsymbol{q},\boldsymbol{\mathcal{K}}_{\rm NN},\epsilon)+H(\boldsymbol{q},\boldsymbol{\mathcal{K}}_{\rm NN},\epsilon)\right](\boldsymbol{\sigma}^{(\mathbf{0})}\cdot\hat{\boldsymbol{\mathcal{K}}})\otimes(\boldsymbol{\sigma}^{(\boldsymbol{i})}\cdot\hat{\boldsymbol{\mathcal{K}}})\\ &+D(\boldsymbol{q},\boldsymbol{\mathcal{K}}_{\rm NN},\epsilon)\left[(\boldsymbol{\sigma}^{(\mathbf{0})}\cdot\hat{\boldsymbol{q}})\otimes(\boldsymbol{\sigma}^{(\boldsymbol{i})}\cdot\hat{\boldsymbol{\mathcal{K}}})+(\boldsymbol{\sigma}^{(\mathbf{0})}\cdot\hat{\boldsymbol{\mathcal{K}}})\otimes(\boldsymbol{\sigma}^{(\boldsymbol{i})}\cdot\hat{\boldsymbol{q}})\right],\end{aligned}\tag{7}$$

where $\boldsymbol{\sigma}^{(\mathbf{0})}$ describes the spin of the projectile, and $\boldsymbol{\sigma}^{(\boldsymbol{i})}$ the spin of the struck nucleon. The average momentum in the NN frame is defined as $\boldsymbol{\mathcal{K}}_{\rm NN}=\frac{1}{2}(\boldsymbol{k}'_{\rm NN}+\boldsymbol{k}_{\rm NN})$. The scalar functions A, C, M, G, H, and D are referred to as Wolfenstein amplitudes, and only depend on the scattering momenta and the energy, and are calculated for np and pp scattering respectively. The amplitude $D(\boldsymbol{q},\boldsymbol{\mathcal{K}}_{\rm NN},\epsilon)$ vanishes on-shell due to parity invariance. Each term in Eq. (7) is described by two components, namely a scalar function of two vector momenta and an energy (for NN scattering this is the c. m. energy of the NN system), and the coupling between the operators of the projectile and the struck nucleon. The Wolfenstein amplitude A sums up all pieces of the central NN force, while C represents all pieces contributing to the spin-orbit force. The amplitudes M, G, and H sum up tensor force contributions.

Evaluating the expectation value of the operator $\mathbf{1}$, (for the struck nucleon i), in the ground state of the nucleus results in the scalar nonlocal, translationally invariant one-body density $\rho_\alpha^{K_s=0}$ in Eq. (1). This has been used successfully as input to microscopic or *ab initio* calculations of leading order effective interactions [14, 16, 21–23]. When evaluation the other operators from Eq. (7), namely $(\boldsymbol{\sigma}^{(\boldsymbol{i})}\cdot\hat{\boldsymbol{n}})$, $(\boldsymbol{\sigma}^{(\boldsymbol{i})}\cdot\hat{\boldsymbol{q}})$, and $(\boldsymbol{\sigma}^{(\boldsymbol{i})}\cdot\hat{\boldsymbol{\mathcal{K}}})$, due to parity invariance arguments only the terms proportional to $(\boldsymbol{\sigma}^{(\boldsymbol{i})}\cdot\hat{\boldsymbol{n}})$ do not vanish in the sum over α for $J^\pi=0^+$ nuclei, leading to spin-projected non-local one-body density $S_{n,\alpha}$ in Eq. (1) [15]. Thus the tensor contributions of the NN force only enter the leading order effective NA interaction through the Wolfenstein amplitude M as long as elastic scattering is considered.

We choose three different chiral NN interactions to study NA observables calculated in leading order of the spectator expansion. One is the optimized chiral NN interaction at the next-to-next-to-leading order NNLO_{opt} from Ref. [1]. This interaction is fitted with $\chi^2\approx 1$ per degree of freedom for laboratory energies up to about 125 MeV. In the A = 3, 4 nucleon systems the contributions of the 3NFs are smaller than in most other parameterizations of chiral interactions.

The second is the chiral NN interaction from Refs. [2, 3] (referred to as EKM) with a semi-local cutoff $R = 1.0$ fm which we consider up to next-to-next-to-leading order. This interaction has been employed in Ref. [20] to quantify truncation errors of the chiral EFT in NA observables. As third interaction we employ the Daejeon16 potential [4], which is based on the Idaho N3LO chiral interaction and is SRG evolved with a flow parameter λ=1.5 fm^{-1} and cast into a harmonic oscillator basis. All three chiral NN interactions describe the np and pp phase shifts equally well for NN laboratory kinetic energies up about 150 MeV, with differences being in details.

We calculated the squares of the real and imaginary parts of the Wolfenstein amplitude A, (sum over the np and pp contributions) for all three interactions, between 65 and 155 MeV laboratory kinetic energies. We considered momentum transfers below 1.6 fm^{-1}, since the forward direction of the amplitude A can be directly related to the differential cross sections for NA scattering at low momentum transfer (small angles) [20]. We noticed that while at the smallest energy (65 MeV) all three potential exhibit roughly the same central strength and agree with the Cd-Bonn calculation, when moving to higher energies the NNLO$_{\rm opt}$ becomes considerably weaker, specifically when extrapolating beyond the energy range included when fitting its low-energy constants. We should thus expect that those differences become visible in NA scattering observables.

Same calculations for the Wolfenstein amplitude C, which characterizes the spin-orbit force of the NN interaction show a different behavior. In general, this amplitude is much smaller in magnitude compared to A (about a factor of 10). We noticed that here even at the lowest energy of 65 MeV, the amplitude C, calculated with the NNLO$_{\rm opt}$ is slightly larger compared to the amplitudes extracted from the other two interactions. This trend increases as the energy increases, indicating that the NN spin-orbit force is slightly stronger in the NNLO$_{\rm opt}$ chiral interaction. The amplitudes C is the main contribution to the spin-orbit part of the NA effective interaction, Eq. (1), and thus it may be expected that its effect may be visible in the NA spin observables.

Tensor force contributions of the NN force are summed up in the Wolfenstein amplitudes M, G, and H. For NA scattering from a 0^+ target, only the amplitude M contributes to the spin-orbit part of the effective interaction. All three chiral interactions considered in this work give identical M amplitudes in the energy range considered and agree perfectly well with the amplitude extracted from the Cd-Bonn potential. A possible explanation may be that the tensor force contributions are determined quite well when fitting to deuteron properties. All NN chiral interactions considered here are fitted to deuteron properties. In addition, the effect of the tensor force contribution to NA spin-observables is quite small in case of scattering from 0^+ targets, as was shown in Ref. [15].

3 Structure and Elastic Scattering Observables

We obtain the ground state energies and wavefunctions of these nuclei by employing the NCSM. In this approach the A-body wavefunctions are expanded in Slater determinants of A single-particle wavefunctions which turns the A-body Schrödinger equation into an eigenvalue problem for the expansion coefficients, with the lowest eigenvalue being the ground state energy. For any finite basis expansion, the obtained eigenvalue, E, gives a strict upper bound for the energy in the complete, but infinite-dimensional basis, and the corresponding eigenvector gives an approximation to the A-body wavefunction. As one increases the basis size, the obtained eigenvalues E approach the exact eigenvalues for a given Hamiltonian.

We follow the standard practice to use a harmonic oscillator (HO) basis for the single-particle wavefunctions, and a truncation parameter $N_{\max}$ is defined as the total number of HO quanta above the minimal configuration for the ground state satisfying the Pauli principle. This leads to an exact factorization of the A-body wavefunction into a center-of-mass wavefunction and a relative wavefunction. We use the ground state wavefunction obtained in the NCSM to evaluate the nonlocal one-body density in single-particle coordinates, from which we subsequently obtain the translationally-invariant nonlocal one-body density [13] that is used as input to the NA scattering calculation [14, 15].

All three nuclei considered here have 0^+ ground states. For ^{4}He and ^{16}O, the most important ground state observables are the energy and the charge radius; while for ^{12}C the quadrupole moment of the first excited state, which is a rotational excitation of the ground state with $J = 2$, also gives information about the deformation. The experimental charge radius is related to the point-proton structure radius via

$$r^2_{\rm str} = r^2_{\rm charge} - \left(R^2_p + \frac{N}{Z} R^2_n + \frac{3}{4m^2_p} \right) , \tag{8}$$

with R^2_p and R^2_n the proton and neutron mean-square charge radii (note that R^2_n is negative) , and m_p is the proton mass.

The NCSM calculations depend on truncation parameters, $N_{\max}$ and the harmonic oscillator $\hbar\omega$. Only in the limit $N_{\max} \to \infty$ the physical observables become independent of $\hbar\omega$. Calculations of ground-state energies and point-proton radius are almost converged for ^{4}He, where $N_{\max} = 18$, but for ^{12}C and ^{16}O, the possible $N_{\max} = 10$ on current computational resources. The radii tend to converge significantly slower. We therefore perform calculations over the range of 16 MeV $< \hbar\omega <$ 24 MeV (15 MeV $< \hbar\omega <$ 25 MeV for Daejeon16), which is a compromise of a common range in which both energy and radii converge rather well.

We present elastic scattering observable for the closed-shell nucleus ^{16}O and open-shell nucleus ^{12}C using the three interactions described previously. In all figures the lines represent the calculations with $\hbar\omega = 20$ MeV, and the

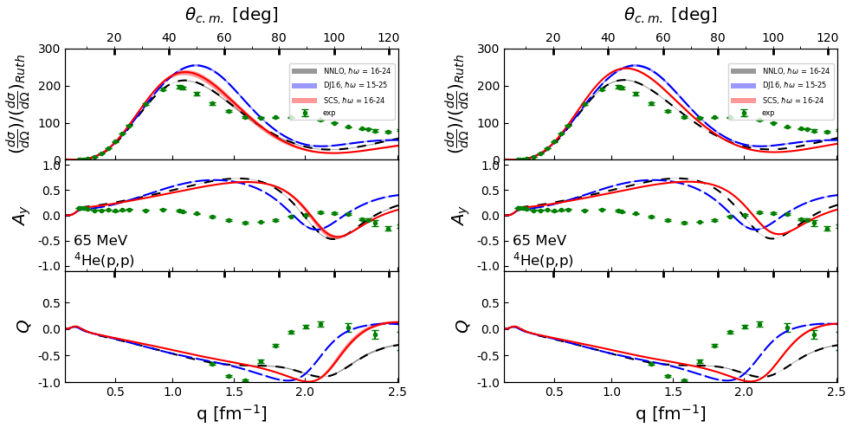

Figure 1. Differential cross section, analyzing power, and spin rotation function, Q, for proton scattering off ^{4}He calculated at 65 MeV projectile energy as function of the transferred momentum q. The calculation employs three interactions: NNLO$_{\rm opt}$ [1] interaction (short-dashed), Daejeon16 [4] interaction (dashed), and EKM [2, 3] interaction (solid) with parameters $\hbar\omega = 20 \pm 4$, and $\mathrm{N_{max}} = 10$ (left) and $\mathrm{N_{max}} = 20$ (right). The experimental data are from Ref. [24] .

bands give the variations in calculations for $\hbar\omega$ in between 16 and 24 MeV for NNL$_{\rm opt}$ and EKM interactions, and in between 15 to 25 MeV for Daejeon16 interaction. The dependence on $\hbar\omega$ results from the calculations of the scalar and spin-projected one-body densities entering the NA effective interactions in leading order in the spectator expansion, and becomes insignificant when $N_{\rm max}$ is large, as it can be seen from Figure 1 where the calculations are performed with $N_{\rm max} = 10$ (left side) and $N_{\rm max} = 20$ (right side). For ^{12}C and ^{16}O, the calculations are performed only up to $N_{\rm max} = 10$ due to large dimensional spaces.

The differential cross sections divided by the Rutherford cross section are calculated at laboratory kinetic energy of 65 MeV where we can compare them with experimental data for ^{12}C from Ref. [24], and for ^{16}O from Ref. [25], in Figure 2. Calculations at laboratory kinetic energy of 100 MeV are presented in Figure 3, and at 160 (180) MeV in Figure 4. The calculated differential cross sections overlap with the experimental values up to momentum transfer values of about 1.2 fm^{-1} at 65 MeV. At 100 MeV, the calculated values are close to the experimental ones for ^{12}C, but they over predict the experimental values for ^{16}O, with calculations based on NNL$_{\rm opt}$ interaction being closer to the experimental data. As we mentioned before, the sum of the square of the real and imaginary part of the Wolfenstein amplitude A (central part) for pp and np scattering, as function of momentum transfer, are almost identical at 65 MeV when calculated with the three interactions, but they start to differ at higher laboratory kinetic

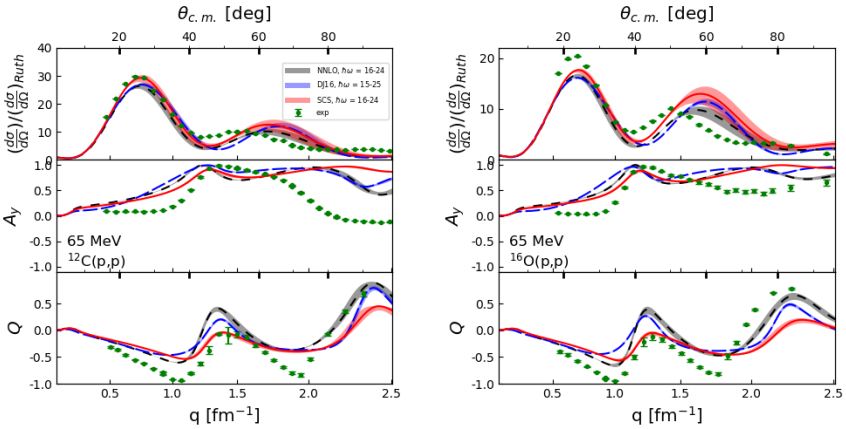

Figure 2. Differential cross section, analyzing power, and spin rotation function, Q, for proton scattering off ^{12}C (left) and ^{16}O (right) calculated at 65 MeV projectile energy as function of the transferred momentum q. The calculation employs three interactions: NNLO$_{\rm opt}$, Daejeon, and EKM interactions with parameters $\hbar\omega = 20 \pm 4$, and $N_{\rm max} = 10$. The experimental data for ^{12}C are from Ref. [24] and for ^{16}O from Ref. [25]. The description of the lines and bands is the same as in Figure 1.

energies. In it interesting to notice that we observe the same behavior in the calculated differential cross sections.

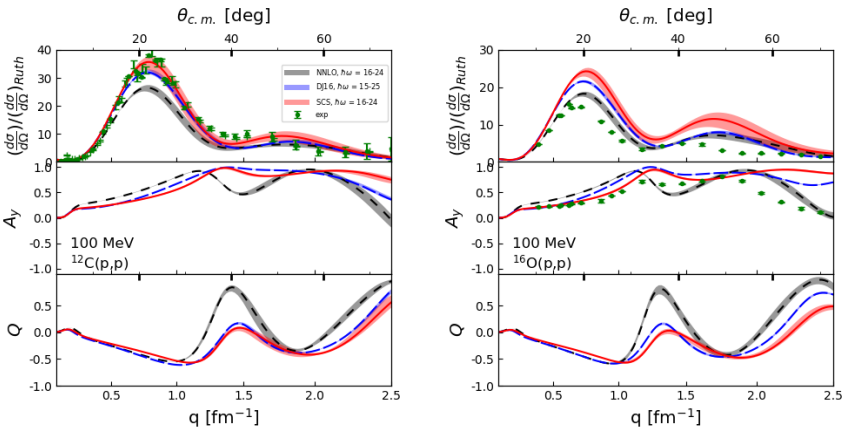

Figure 3. Differential cross section, analyzing power, and spin rotation function, Q, for proton scattering off ^{12}C and ^{16}O calculated at 100 MeV projectile energy as function of the transferred momentum q. The calculation employs several interactions: NNLO$_{\rm opt}$, Daejeon, and EKM interactions with parameters $\hbar\omega = 20 \pm 4$, and $N_{\rm max} = 10$. The description of the lines and bands is the same as in Figure 1.

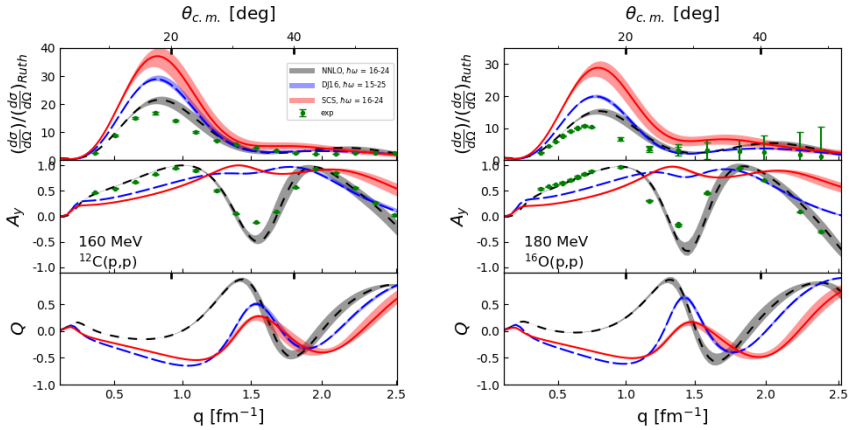

Figure 4. Differential cross section, analyzing power, and spin rotation function, Q, for proton scattering off ^{12}C at 160 MeV [27], and ^{16}O calculated at 180 MeV [28] projectile energy as function of the transferred momentum q. The calculation employs several interactions: NNLO$_{\rm opt}$, Daejeon, and EKM interactions with parameters h$\omega = 20 \pm 4$, and N$_{\rm max} = 10$. The description of the lines and bands is the same as in Figure 1.

As we discussed in Section 2, the Wolfenstein amplitude C, characterizes the spin-orbit force of he NN interaction, and calculated with the three interactions, has different values with the highest with NNLO$_{\rm opt}$, and lowest with EKM, and the differences increase with increasing laboratory kinetic energy. It is interesting to notice that we observe a similar pattens in calculations of the analyzing power, A_y, and the spin rotation function, Q. The calculated A_y and Q are similar at 65 MeV with differences at higher momentum transfer values. At 100 MeV, and 160 (180) MeV, the calculations with NNLO$_{\rm opt}$ interaction describe well the A_y values for ^{12}C and ^{16}O, while the Daejeon16 and EKM interactions are missing the dip in A_y at about 1.5 fm^{-1}. There are less available experimental data for spin rotation function Q. Calculated values predict similar results at low momentum transfer with all three interactions, but they start to differ about about 1 fm^{-1} with increased laboratory kinetic energy. More details are presented in our recent paper [26].

4 Conclusion

In this work we calculated elastic scattering observables for ^{4}He, ^{12}C and ^{16}O in an *ab initio* framework for three different NN interactions based on chiral effective field theory. As examples, we studied the open-shell nucleus ^{12}C and the close-shell nucleus ^{16}O. The elastic scattering observables are calculated using the leading order in the spectator expansion, so two nucleons are active in the scattering process. Since the NCSM calculations depend on the parameters $N_{\rm max}$ and $\hbar\omega$, we used the highest possible value of $N_{\rm max}$ for each nucleus, and

we choose the $\hbar\omega$ for which the ground state energy and the point-proton radii are close to convergence. Our study shows that the three NN interactions based on a chiral field theory framework and calibrated to reproduce similar data in the few-nucleon systems, predict NA scattering observables quite differently.

Acknowledgements

This work was performed in part under the auspices of the U.S. Department of Energy under contract Nos. DE-FG02-93ER40756 and DE-SC0023495. The numerical computations benefited from computing resources provided by the National Energy Research Scientific Computing Center (NERSC), a U. S. DOE Office of Science User Facility located at Lawrence Berkeley National Laboratory, operated under contract No. DE-AC02-05CH11231. G.P. acknowledges the support from the Ohio University Zanesville.

References

[1] A. Ekström *et al.*, *Phys. Rev. Lett.* **110** (2013) 192502.
[2] E. Epelbaum, H. Krebs, U.G. Meißner, *Phys. Rev. Lett.* **115** (2015) 122301.
[3] E. Epelbaum, H. Krebs, U.G. Meißner, *Eur. Phys. J. A* **51** (2015) 53.
[4] A.M. Shirokov, I.J. Shin, Y. Kim, M. Sosonkina, P. Maris, J.P. Vary, *Phys. Lett. B* **761** (2016) 87.
[5] P. Navratil, J.P. Vary, B.R. Barrett, *Phys. Rev. Lett.* **84** (2000) 5728.
[6] P. Navratil, J.P. Vary, B.R. Barrett, *Phys. Rev. C* **62** (2000) 054311.
[7] R. Roth, P. Navratil, *Phys. Rev. Lett.* **99** (2007) 092501, arXiv:0705.4069.
[8] B. Barrett, P. Navrátil, J. Vary, *Prog. Part. Nucl. Phys.* **69** (2013) 131.
[9] C. Stumpf, J. Braun, R. Roth, *Phys. Rev. C* **93** (2016) 021301.
[10] E.R. Siciliano, R.M. Thaler, *Phys. Rev. C* **16** (1977) 1322.
[11] A. Picklesimer, P.C. Tandy, R.M. Thaler, *Ann. Phys.* **145** (1983) 207-307.
[12] R.B. Baker, M. Burrows, C. Elster, K.D. Launey, P. Maris, G. Popa, S. Weppner, *Front. Phys.* **10** (2023) 1071971.
[13] M. Burrows, C. Elster, G. Popa, K.D. Launey, A. Nogga, P. Maris, *Phys. Rev. C* **97** (2018) 024325.
[14] M. Burrows, C. Elster, S. Weppner, K.D. Launey, P. Maris, A. Nogga, G. Popa, *Phys. Rev. C* **99** (2019) 044603.
[15] M. Burrows, R.B. Baker, C. Elster, S. Weppner, K.D. Launey, P. Maris, G. Popa, *Phys. Rev. C* **103** (2021) 054313.
[16] M. Gennari *et al.*, *Phys. Rev. C* **97** (2018) 024325.
[17] M. Vorabbi *et al.*, *Phys. Rev. C* **105** (2022) 014621.
[18] C. Møller, K. Dan, *Vidensk. Sels. Mat. Fys. Medd.* **23** (1945) 1.
[19] L. Wolfenstein, J. Ashkin, *Phys. Rev.* **85** (1952) 947.
[20] R.B. Baker *et al.*, *Phys. Rev. C* **106** (2022) 064605.
[21] Ch. Elster, T. Cheon, E.F. Redish, P.C. Tandy, *Phys. Rev. C* **41** (1990) 814.
[22] Ch. Elster, S.P. Weppner, C.R. Chinn, *Phys. Rev. C* **56** (1997) 2080.
[23] H.F. Arellano, G. Blanchon, *Phys. Rev. C* **98** (2018) 054616.

[24] M. Ieiri *et al.*, *Nucl. Instrum. Meth. Phys. Res. A* **257** (1987) 253.

[25] H. Sakaguchi *et al.*, *Phys. Lett. B* **89** (1979) 40.

[26] R.B. Baker, M. Burrows, C. Elster, P. Maris, G. Popa, S. Weppner, *Phys. Rev. C* **108** (2023) 044617.

[27] H.O. Meyer *et al.*, *Phys. Rev. C* **27** (1983) 459.

[28] J.J. Kelly *et al.*, *Phys. Rev. C* **41** (1990) 2504.